Photocatalytic Degradation of Aqueous Nitrobenzene by Nanocrystalline TiO 2

ARTICLE *in* INDUSTRIAL & ENGINEERING CHEMISTRY RESEARCH · FEBRUARY 2006

Impact Factor: 2.59 · DOI: 10.1021/ie051060m

Photocatalytic Degradation of Aqueous Nitrobenzene by Nanocrystalline TiO_2

Rajesh J. Tayade,[†] Ramchandra G. Kulkarni,[‡] and Raksh. V. Jasra*[,†]

Silicates and Catalysis Discipline, Central Salt & Marine Chemicals Research Institute, G. B. Marg, Bhavnagar 364002, India, and Department of Physics, Saurashtra University, Rajkot 360005, India

This study investigated the role of the band gap, surface area, and phase composition on the photocatalytic activity of nanocrystalline TiO_2. Nanocrystalline TiO_2 (8−29 nm) was synthesized by hydrolysis of titanium tetraisopropoxide. The crystalline structure, band gap, and morphology of the nanocrystalline TiO_2 were determined by X-ray diffraction (XRD), diffuse reflectance spectroscopy (DRS), and N_2 adsorption (BET) at 77 K, respectively. It is observed that the band gap of the nanocrystalline TiO_2 decreases from 3.29 to 3.01 eV with increasing calcination temperature. The crystallite size of the TiO_2 samples prepared also shows an increase with increasing calcination temperature. The photocatalytic degradation of an aqueous solution of nitrobenzene (50 ppm) was studied using nanocrystalline TiO_2 samples with varying band-gap values, as well as a P-25 Degussa TiO_2 sample for comparison. The initial rate of degradation of nitrobenzene was calculated in each case to evaluate the photocatalytic activity of the catalysts. The enhanced photocatalytic degradation of nitrobenzene was observed by purging air through the solution during photocatalysis.

Introduction

Nitrobenzene has been nominated by the National Institute of Environmental Health Sciences for listing in the Report on Carcinogens based on the conclusions of an International Agency for Research on Cancer (IARC). The U.S. Environmental Protection Agency (EPA) recommends[2] that levels in lakes and streams should be limited to 17 parts of nitrobenzene per million parts of water (17 ppm) to prevent possible health effects from drinking water or eating fish contaminated with nitrobenzene. The U.S. Occupational Safety and Health Administration (OSHA) has set[2] a permissible exposure limit of 5 mg of nitrobenzene per cubic meter of air (5 mg/m^3) for an 8-h workday in a 40-h work week. A small amount of nitrobenzene can cause mild irritation if it contacts the skin or eyes directly. However, repeated exposures to a high concentration of nitrobenzene can result in methemoglobinemia, a condition in which the blood's ability to carry oxygen is reduced. It has been estimated that about 19 million lb of nitrobenzene is released into the environment annually.[1] Nitrobenzene is released into the environment mainly by industries, but it can also form in the atmosphere through the nitration of benzene, a common air pollutant. However, the largest source of nitrobenzene release is its manufacture and use as a chemical intermediate in the synthesis of aniline. Smaller amounts are also released from consumer products in which nitrobenzene is used as a solvent. The highest concentration of nitrobenzene is reported in wastewater from the organics and plastics industries, with some reported levels exceeding 100 ppm (ATSDR, 1990).[2] Nitrobenzene is degradable by anaerobic processes. However, such processes are very slow. For example, Chou et al.[3] reported that nitrobenzene was removed to the extent of 81% in 110 days by acclimated domestic sludge in an anaerobic reactor, and Hallas and Alexander[4] found that 50% was degraded in 12 days under similar conditions. Canton et al.[5] measured an 8% decrease in nitrobenzene after 8 days in unadapted media, but reported a half-life of less than 2 weeks in adapted media.

Nitrobenzene was reported to be either highly resistant to degradation or to inhibit the biodegradation of other components of the waste in several biodegradation studies.[6−10] However, these effects were observed at concentrations (≥50 mg/L) of nitrobenzene much higher than those detected in ambient waters. The degradation of nitrobenzene by different irradiation sources has been studied by Rodriguez et al.,[11] who achieved total organic content removals of 53%, 60%, and 76% by irradiation with 253.7-nm UV light, a Xe lamp, and solar light, respectively. No effect was observed during direct photolysis of nitrobenzene with a 150-W mercury−xenon lamp in the study carried out by Lipczynska-Kochany.[12] The degradation of nitrobenzene in aqueous solution by a O_3/UV advanced oxidation process and a UV/Fe(III)-enhanced ozonation process was studied by Contreras et al.[13] The photocatalytic degradation of nitrobenzene using concentrated solar radiation in a novel photocatalytic reactor was studied by Kamble et al.[14] Degradation of nitrobenzene was also studied by Bhatkhande et al.[15,16] with an advanced photocatalytic oxidation process using concentrated sunlight and artificial ultraviolet light.

Photocatalysis using semiconductors such as TiO_2 has been demonstrated to be an inexpensive and effective method for treating a wide range of pollutants, including alkanes, alcohols, carboxylic acids, alkenes, phenols, dyes, PCBs, aromatic hydrocarbons, halogenated alkanes, surfactant, and pesticides, in both water and air.[17−24] Therefore, in the present study, the decomposition of an aqueous solution of nitrobenzene using nanocrystalline TiO_2 samples of different band gaps as photocatalysts was studied. Nitrobenzene was selected for investigation because of its high occurrence in industrial wastewater, as well as its quite low reactivity toward biochemical/chemical oxidation.

Many studies have been carried out on the photocatalytic activity of nanocrystalline TiO_2 for the degradation of organic compounds, but here, we have tried to investigate the photocatalytic activity of nanocrystalline TiO_2 samples with varied band gaps and also to study the effect of the TiO_2 calcination temperature on its crystallite size, band gap, and surface area, as well as the photocatalytic degradation of nitrobenzene.

Experimental Section

Chemicals and Reagents. Titanium(IV) isopropoxide (97%) was obtained from Aldrich (Milwaukee, WI). Nitrobenzene, AR grade (99.0%), was procured from S.D. Fine-Chem Ltd.

* To whom correspondence should be addressed. E-mail: rvjasra@csmcri.org. Fax: +91 278 2567562. Tel.: +91 278 2471793.

[†] Central Salt & Marine Chemicals Research Institute.

[‡] Saurashtra University.

10.1021/ie051060m CCC: $33.50
Published on Web 01/05/2006

(Mumbai, India). Titanium dioxide (P-25) was purchased from Degussa Corporation (Degussa AG, Frankfurt, Germany). COD Standard chemical reagents for chemical oxygen demand (COD) measurements were purchased from E. Merck India Limited (Darmstadt, Germany).

Synthesis of Nanocrystalline TiO_2. Nanocrystalline TiO_2 was synthesized by hydrolysis of titanium tetraisopropoxide. A mixture of dry ethanol (100 mL) and titanium tetraisopropoxide (30 mL) was taken in a 250 mL round-bottom flask, continuously stirred for 30 min, and then subjected to ultrasonication for 30 min. Hydrolysis of the titanium tetraisopropoxide solution was carried out by adding distilled water (24 mL) slowly at the rate of 0.5 mL/min with continuous stirring. The solvent from the obtained mixture was removed using a rotavapor apparatus (Buchi, R-205) at 343 K under reduced pressure. The powder was then kept in an oven at 393 K overnight. The sample thus obtained is identified as NCT-393. The dried sample was calcined at different temperatures (i.e., 583, 673, 753, 833, 913, and 1023 K) under air for 11 h, and the calcined samples are identified as NCT-583, NCT-673, NCT-753, NCT-833, NCT-913, and NCT-1023, respectively, with numbers denoting the calcination temperature in Kelvin. The calcination was carried out in a tubular furnace under a flow of air (flow rate =3 L/min) to 913 K. Sample NCT-1023 was calcined in a muffle furnace without an airflow.

Catalyst Characterization. Powder X-ray diffraction patterns were recorded with a Phillips X'pert MPD system using Cu Kα radiation ($\lambda = 0.15405$ nm) in a 2θ range of 5−60° at a scan speed of 0.1° s^{-1}. The obtained X-ray diffraction patterns were compared with the standard anatase and rutile diffractograms.[25] The phase percentage formed was determined from the integrated intensity peak at $2\theta = 25.3°$ (101) for anatase and $2\theta = 27.4°$ (110) for rutile. The percentage of anatase, *A*, was determined using eq 1[26]

$$A\,(\%) = 100/(1 + 1.265I_R/I_A) \tag{1}$$

where I_R is the intensity of the rutile peak at $2\theta = 27.4°$ and I_A is the intensity of the anatase peak at $2\theta = 25.3°$.

Crystallite sizes of samples were calculated from the widths at half-height of different peaks of anatase using the Scherrer equation

$$\text{crystallite size} = K\lambda/W\cos\theta \tag{2}$$

with $W = W_b - W_s$, where W_b is the broadened profile width of the experimental sample and W_s is the standard profile width of the reference sample, λ is the wavelength of X-ray radiation (Cu Kα = 0.15405 nm), and θ is the diffraction angle. Characteristic peaks at $2\theta = 25.3°$ (101) for anatase and $2\theta = 27.4°$ (110) for rutile using the Scherrer formula with a shape factor[27] (*K*) of 0.9 were employed. High-purity silicon was used as an internal standard to account for the effect of instrumental line broadening during crystal size determinations.

Specific surface areas, pore volumes, and pore size distributions of the calcined samples were determined from N_2 adsorption−desorption isotherms at 77 K (ASAP 2010, Micromeritics, Norcross, GA). Surface areas and pore size distributions were determined using the BET equation and BJH method, respectively.[28] The samples were degassed under vacuum (10^{-3} Torr) at temperatures below their calcination temperature for 4 h, prior to measurements. Samples NCT-393 and NCT-583 were degassed at 373 and 573 K, respectively, whereas samples NCT-673, NCT-753, NCT-833, NCT-913, NCT-1023, and P-25 Degussa were degassed at 623 K.

The band-gap energy of the nanocrystalline TiO_2 was determined using diffuse reflectance spectroscopy (DRS) on an instrument (Shimadzu UV-3101PC) equipped with an integrating sphere and with $BaSO_4$ as a reference.[29−31] The spectra were recorded at room temperature in the wavelength range of 250−600 nm. The band-gap energies of the catalysts and P-25 Degussa standard were determined using the DR−UV−vis method and calculated according to eq 3

$$\text{band gap (EG)} = hc/\lambda \tag{3}$$

where EG is the band-gap energy (eV), *h* is Planck's constant, *c* is the speed of light (m/s), and λ is the wavelength (nm).

A scanning electron microscope (Leo series VP1430) was used to determine the morphology of the catalyst samples after calcination at different temperatures. The sample powders were supported on aluminum stubs using silver paint and then coated with gold by plasma prior to measurements.

Photocatalytic Irradiation System. The photocatalytic activities of nanocrystalline TiO_2 samples calcined at various temperatures were determined by studying the decomposition of an aqueous solution of nitrobenzene (50 ppm) in a photocatalytic reactor. The photocatalytic reactor consisted of two parts. The first part was an inner quartz double-wall jacket with an inlet and outlet for water circulation to maintain the temperature of the reaction mixture. This jacket had an empty chamber at the center for the immersion of a 125-W mercury vapor lamp (Crompton, high-pressure mercury vapor lamp, with the glass bulb removed) used for irradiation of the reaction mixture. The second part was an outer borosilicate glass container (volume of 250 mL after insertion of the inner part) in which the aqueous solution was taken and irradiated. It was cooled by water circulation to room temperature during experiments. The concentration of substrate in the bulk solution prior to irradiation was used as the initial value for the measurements of nitrobenzene degradation. At each interval of 1 h, a 5-mL sample was withdrawn by syringe from the irradiated suspension. The catalyst was separated by centrifuge from the aqueous solution prior to analysis. Before commencing irradiation, a suspension containing 50 mg of the catalyst and 250 mL of an aqueous solution of about 50 ppm nitrobenzene was ultrasonicated for 2 min and then stirred for 30 min in the dark; to determine the adsorption on the catalyst, a 10-mL sample was withdrawn by syringe for analysis.

Chemical Analysis. The UV−visible absorbance of aqueous solutions of nitrobenzene was measured at $\lambda_{max} = 268$ nm with a Cary 500 UV−vis spectrophotometer (Varian, Palo Alto, CA), equipped with a quartz cell having a path length of 1 cm. The spectral absorbance was measured with baseline correction at scan rate of 600 nm min^{-1} and a data-point interval of 1 nm. The concentration of nitrobenzene in the solution was determined using a calibration curve of nitrobenzene (concentration vs absorbance) prepared with known concentrations.

The oxygen equivalent of the organic matter of each sample, i.e., chemical oxygen demand (COD), was measured using a Spectroquant NOVA 60 photometer (Merck KGaA, Darmstadt, Germany). The reagents for COD analysis and a 3-mL sample taken at a specific time were mixed together in a glass cell and digested in a Spectroquant TR 320 Thermodigester for 2 h at 148 °C. After digestion, the mixture was cooled to room temperature, and the COD was measured using the photometer. The COD was measured for the original solution and for centrifuged samples withdrawn at different time intervals.

Results and Discussion

Crystallinity and Crystallite Size. The X-ray diffraction patterns of nanocrystalline TiO_2 samples calcined at different temperatures are shown in Figure 1. The crystallite sizes of

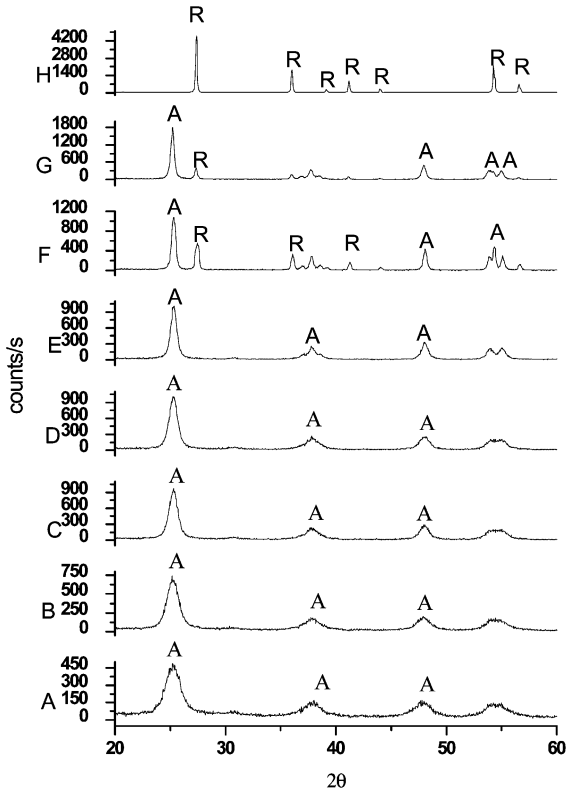

Figure 1. XRD patterns of nanocrystalline TiO_2 samples calcined at different temperatures: (A) NCT-393, (B) NCT-583, (C) NCT-673, (D) NCT-753, (E) NCT-833, (F) NCT-913, (G) P-25, (H) NCT-1023.

Table 1. Textural and Electronic Properties of Synthesized Nanocrystalline TiO_2 Samples

catalyst	BET surface area ($m^2\ g^{-1}$)	average pore volume ($cm^3\ g^{-1}$)	average pore diameter (Å)	anatase crystallite size (nm)	band edge (nm)	band gap (eV)
NCT-393	259	0.310	48	08	376.4	3.30
NCT-583	199	0.300	61	09	376.5	3.29
NCT-673	166	0.280	67	12	378.5	3.28
NCT-753	124	0.230	75	14	400.0	3.04
NCT-833	091	0.170	76	19	400.2	3.1
NCT-913	002	0.004	73	29	408.0	3.03
NCT-1023	002	0.005	54	–	411.9	3.01
P-25	061	0.120	82	28	393.7	3.15

various samples determined from XRD using eq 2 are reported in Table 1. XRD data show that the synthesized TiO_2 samples are nanocrystalline, with crystallite sizes varying from 8 to 29 nm and with higher increases in size observed after calcination. A similar increase in crystallite size with increasing calcination temperature was also reported by Kim et al.[32] for nanocrystalline TiO_2 prepared by the hydrolysis of titanium tetraisopropoxide in the aqueous cores of water/NP-5/cyclohexane microemulsions.

Prior to calcination, the prepared TiO_2 powder was largely amorphous in nature. The phase transformation from anatase to rutile started at 913 K and was complete at 1023 K. As the temperature of calcination was increased, the crystallite size was also found to increase. The nanocrystalline TiO_2 samples calcined at 583−833 K were anatase in nature. Chen et al.[33] reported the synthesis of nanocrystalline TiO_2 by the hydrolysis of titanium tetraisopropoxide in aqueous solutions of varying pH and the formation of anatase powder at calcination temperatures of 523−723 K. They reported the formation of a rutile phase to occur above 873 K, with an increase in crystallite size as the calcination temperature increased. Such a crystal phase

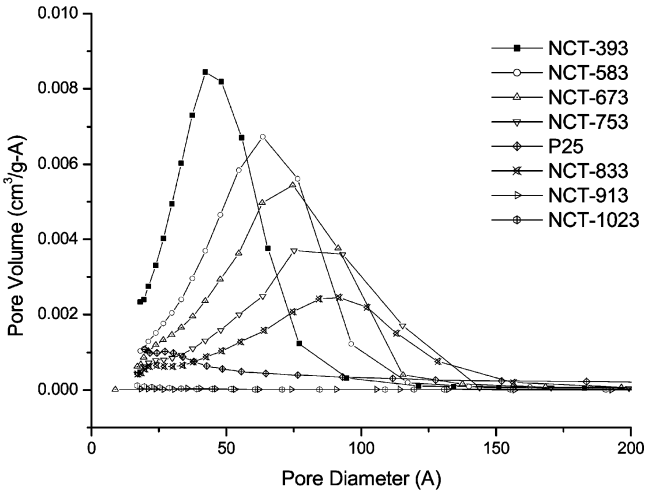

Figure 2. Pore size distributions for nanocrystalline TiO_2 samples calcined at various temperatures.

transformation upon calcination of TiO_2 powder at higher temperature is known to occur. It has been further reported that amorphous-to-anatase and anatase-to-rutile phase transformations depend strongly on the method of preparation, the nature of the precursor, and the calcination conditions.[32,33] Comparison of our data with those of Chen et al.[33] shows that the anatase-to-rutile conversion occurs at higher temperature (913 K) for nanocrystalline material than for bulk TiO_2 (873 K).

Textural Properties. N_2 adsorption isotherms measured at 77 K were of type IV typically observed for mesoporous solids. The adsorption isotherms for the samples obtained after calcination at 913 and 1023 K were of type III, reflecting marginal porosity. The surface areas and pore volumes of the nano-TiO_2 samples calcined at various temperatures are reported in Table 1. The pore size distributions for nanocrystalline TiO_2 after calcination at different temperatures are shown in Figure 2. It is observed from this figure that the pore size distribution broadens and the average pore diameter increases with increasing calcination temperature. The sample synthesized at 393 K has the highest surface area, 259 $m^2\ g^{-1}$, and the smallest crystallite size of 8 nm. However, calcination at higher temperatures significantly affects the textural properties of the nanocrystalline TiO_2. For example, the 259 $m^2\ g^{-1}$ surface area of the prepared amorphous TiO_2 powder was reduced to 2 $m^2\ g^{-1}$ through the increase in the calcination temperature. The high surface area observed for the dried and amorphous sample is due to its textural character, with weakly aggregated TiO_2 particles that give rise to mesoporosity. Upon calcination, crystalline phases develop, resulting in a denser packing of the particles and a reduction of the porosity of the samples. The nanocrystalline TiO_2 sample NCT-833 was observed to have the maximum content of anatase phase and had a surface area of 91 $m^2\ g^{-1}$. The surface areas of nanocrystalline TiO_2 samples containing both anatase and rutile phase were very low at 2 $m^2\ g^{-1}$. The sharp decrease in pore volume obtained at 913 K is because of sintering, which indicates the formation of a densely packed crystalline structure of nano-TiO_2. The nanocrystalline TiO_2 sample prepared in this study having the highest photoactivity is NCT-753, which has a surface area of 124 $m^2\ g^{-1}$ and an average pore diameter of 75 Å.

Electronic Properties. DRS spectra and their differential curves for nanocrystalline TiO_2 samples are shown in Figure 3a and b, respectively. Comparing these spectra, a shift toward longer wavelength of 35.5 nm was observed for NCT-1023 compared to that for NCT-393. To obtain more precise band edges for these semiconductor powders, a differential calculation

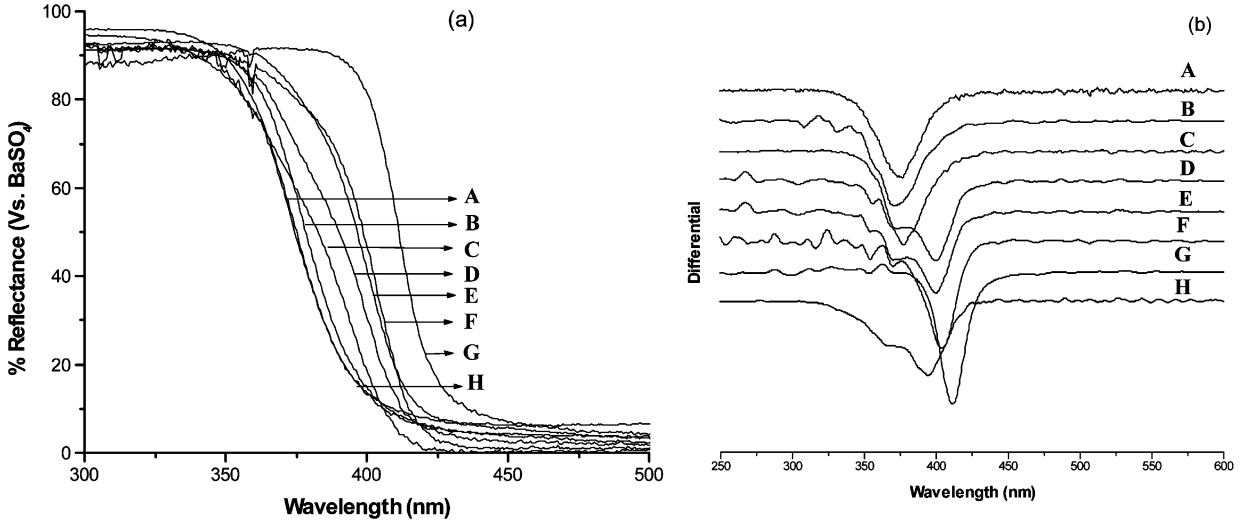

Figure 3. (a) DRS spectra of nanocrystalline TiO_2 samples calcined at the temperatures of (A) 393, (B) 583, (C) 673, (D) 753, (E) 833, (F) 913, and (G) 1023 K and (H) P-25 Degussa. (b) Band-gap measurements using differentiation calculations of DRS spectra for different TiO_2 samples.

was done, and the resulting curves are shown in Figure 3b. The band edges of the samples determined from differentiation of all of the curves are reported in Table 1. The band gap of the amorphous NCT-393 sample is 3.29 eV. Upon heat treatment, the amorphous TiO_2 converts to the anatase phase, and the band gap decreases from 3.29 to 3.1 eV at 833 K. The crystallite size of anatase nanocrystalline TiO_2 increases with increasing calcination temperature. There is a sharp decrease in band gap in the temperature range from 673 to 913 K. The change in band-gap values could be due to the change in the nature and crystalline phase of TiO_2, as well as in its crystallinity, with calcination temperature. Another factor that might contribute to the decrease in band-gap value is the smaller crystallite size of the semiconductor, probably owing to a quantum size effect, observed at higher temperature. The band gap of the nanocrystalline TiO_2 rutile prepared by us is 3.01 eV.

Morphology. Micrographs of the TiO_2 samples (Figure 4) show a globular morphology of the particles. Sintering of the particles is clearly observed with increasing calcination temperature.

Photocatalytic Activity. The photoactivity of the prepared TiO_2 particles was investigated using the degradation of aqueous nitrobenzene solution. The photocatalytic activity values for all of the samples prepared at different calcination temperatures are as reported in Table 2. The catalysts studied are NCT-583, NCT-673, NCT-753, NCT-833, NCT-913, NCT-1023, P-25, and a mixture of NCT-833 and NCT-1023 in an 8:2 ratio (denoted as NCT-AR). It is observed that the extents of adsorption of nitrobenzene from aqueous solution on catalysts NCT-583, NCT-673, NCT-753, NCT-833, NCT-913, NCT-1023, and NCT-AR were 10%, 9%, 8%, 6%, 3%, 2%, 2%, and 5%, respectively, and the adsorption of nitrobenzene on P-25 was 9%. The adsorption data show that the adsorption decreases as the TiO_2 calcination temperature increases. This is mainly due to the decrease in surface area observed with increasing calcination temperature. The band gaps for the NCT-583, NCT-673, NCT-753, NCT-833, NCT- 913, NCT-1023, NCT-AR, and P-25 samples are 3.29, 3.29, 3.28, 3.10, 3.02, 3.02, 3.01, 3.05, and 3.15 eV, respectively. As seen in Table 2, the highest activity is shown by NCT-753, as reflected in both the UV−vis spectra and COD data. UV−vis spectra of an aqueous solution of nitrobenzene collected at different reaction times for the NCT-753 sample are shown in Figure 5. Similar UV−vis spectra were observed for the other samples. The nanocrystalline TiO_2 sample NCT-833 has a crystallite size of 16 nm. It displayed bandgap of 3.1 eV among the nanocrystalline TiO_2 samples prepared and contains nearly 100% anatase, but its photoactivity is lower than that of NCT-753. This could be due to the higher surface area and decreased recombination of electron−hole pairs in the case of NCT-753 as compared to NCT-833. Usually, the composite of two kinds of semiconduc-

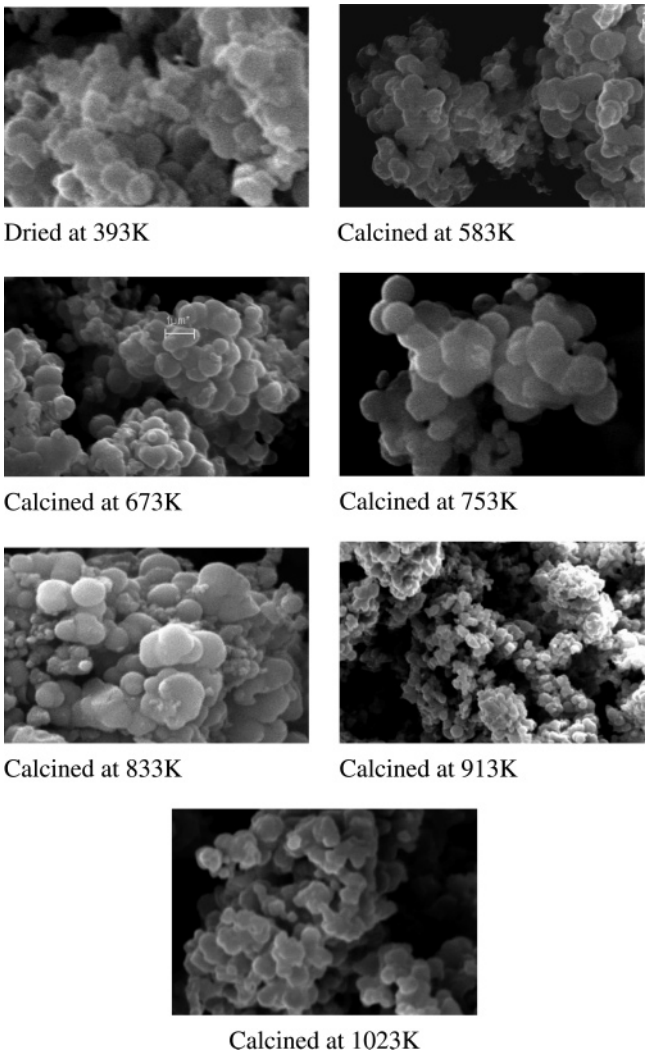

Figure 4. SEM images of nanocrystalline TiO_2 samples calcined at different temperatures.

Table 2. Degradation of Nitrobenzene with Irradiation Time Using Catalysts Calcined at Various Temperatures[a,b]

	1 h		2 h		3 h		4 h		5 h		6 h		7 h		8 h	
catalyst	A	B	A	B	A	B	A	B	A	B	A	B	A	B	A	B
NCT-583	44	65	60	88	75	42	81	35	87	32	91	28	94	20	94	19
NCT-673	54	45	70	88	77	53	83	47	88	32	91	38	94	24	96	16
NCT-753	59	68	76	56	86	54	90	34	94	28	96	25	97	20	98	10
NCT-833	51	60	68	55	74	53	79	26	82	28	84	22	87	18	88	12
NCT-913	52	59	66	57	75	38	86	24	92	23	95	20	96	15	97	12
NCT-1023	49	62	63	58	70	56	74	54	76	22	77	44	79	40	81	42
P-25	57	62	72	57	80	44	87	38	90	48	92	26	94	21	95	18

[a] Initial concentration of nitrobenzene = 50 ppm. Initial COD value of nitrobenzene (50 ppm) = 96 mg L^{-1}. Blank COD value = 6 mg L^{-1}. [b] A = Percent degradation of nitrobenzene determined by UV−vis spectrophotometry. B = COD value of reaction mixture.

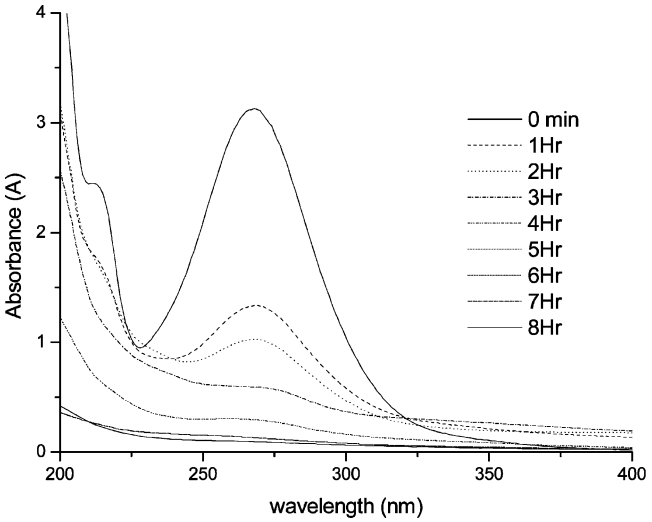

Figure 5. UV spectra of aqueous solutions of nitrobenzene after treatment with TiO_2 sample NCT-753.

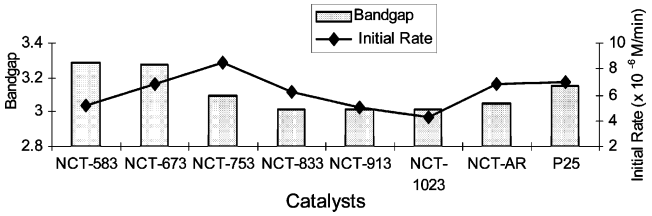

Figure 6. Initial rates of degradation of aqueous nitrobenzene solutions and band gaps of nanocrystalline TiO_2 samples calcined at different temperatures.

tors or two phases of semiconductor is beneficial in reducing the combination of photogenerated electrons and holes, thereby enhancing the photocatalytic activity. It is reported that catalysts containing only anatase or only rutile are less efficient than catalysts that contain both phases.[33] The initial rates of degradation of nitrobenzene using various catalysts and their band gaps are shown in Figure 6. The maximum initial rate of degradation of nitrobenzene was obtained using sample NCT-753. This might be because of the higher surface area of 124 m^2/g, low crystallite size of 14 nm, and lower band gap as compared to the standard P-25 Degussa (band gap = 3.15 eV). Baolong et al.[35] reported that a catalyst prepared by them using monomer droplet templates had a high surface area of 87 m^2/g and exhibited a high photodegradation of KN-R dye.

It was also observed that the initial rate of photocatalytic degradation of nitrobenzene for the NCT-913 sample, which had the lowest band gap (3.03 eV, surface area = 2 m^2 g^{-1}) among the prepared nanocrystalline TiO_2 samples containing both anatase and rutile phases, was higher than those of NCT-833 (band gap = 3.1 eV, surface area = 91 m^2 g^{-1}) and NCT-1023 (band gap = 3.01 eV, surface area = 2 m^2 g^{-1}). This indicates that the minimum band gap of the catalyst in the anatase phase is helpful to achieving a higher degradation of nitrobenzene and that the minimum band gap in the rutile phase is not helpful for achieving a higher photocatalytic degradation. It has been reported that the rutile phase of TiO_2 is less active than the anatase phase for the degradation of organic compounds because the rutile phase has a slight lower Fermi level, a closed structure, and a low degree of surface hydroxylation. In our study also, NCT-1023, which is completely rutile, showed a lower activity than the other catalysts calcined at different temperatures.

Table 3. Degradation of Nitrobenzene with Irradiation Time Using Catalysts Calcined at Various Temperatures with Air Purge[a,b]

	1 h		2 h		3 h		4 h	
catalyst	A	B	A	B	A	B	A	B
NCT-583	87.1	24	99.3	08	100	00	100	00
NCT-673	91.1	22	99.7	06	100	00	100	00
NCT-753	86.9	18	99.5	00	100	00	100	00
NCT-833	87.1	24	98.5	10	100	00	100	00
NCT-913	86.2	24	98.1	12	100	00	100	00
NCT-1023	80.0	34	86.5	22	90.5	14	99.3	00
P-25	90.1	20	99.8	00	100	00	100	00

[a] Initial concentration of nitrobenzene = 50 ppm. Initial COD value of nitrobenzene (50 ppm) = 96 mg L^{-1}. Blank COD value = 6 mg L^{-1}. [b] A = Percent degradation of nitrobenzene determined by UV−vis spectrophotometry. B = COD value of reaction mixture.

In photocatalytic degradation, the generation and migration of the photogenerated electron−hole pair and the reaction between photogenerated holes (or hydroxyl radical) and organic compounds are two processes that occurs in series. Therefore, each step can become rate-determining for the overall process. The initial rate of degradation of nitrobenzene increases with increasing calcination temperature of the TiO_2 catalyst, probably because of the transformation from an amorphous phase to anatase and a decrease in the band gap of the nanocrystalline TiO_2, which helps the generation of electron−hole pairs in anatase. Thus, it is clear that, because of the high surface area and low recombination of electron−hole pairs, the extent of degradation is greater. The initial COD of the 50 ppm nitrobenzene solution was 96 mg L^{-1}, which decreased to 10 mg L^{-1} upon 8 h of irradiation without purging air. It was observed that the COD values decreased for NCT-583 and NCT-673 during the first hour and then increased during the subsequent 2 h, which again starts decreasing, as reported in Table 2.

Effect of Air Purge during Degradation of Nitrobenzene. In the present study, it can be seen in Table 3 that, with an air purge at a rate of 2 L/min, the photocatalytic degradation of nitrobenzene increased, and the total degradation of nitrobenzene was obtained in 2 h. The highest activity was obtained for NCT-753 with an air purge. Tables 2 and 3 show the percentage of degradation of nitrobenzene with purging of air and without air. For the continuation of the photocatalytic oxidation of organic compounds, it is necessary to remove the photogenerated electrons, which can be done by using an electron acceptor such as oxygen that is easily available during purging with air. Wang

et al.[36] also observed similar photocatalytic activities for the decomposition of organic compounds in the presence of oxygen.

Conclusions

Nanocrystalline TiO_2 samples of various band gaps were prepared by the hydrolysis of titanium isopropoxide. The band gap of nanocrystalline TiO_2 changes with increasing calcination temperature and particle crystallite size. The band gap of the semiconductor and the phase composition play major roles in the photodegradation of nitrobenzene. The nanocrystalline TiO_2 samples containing amorphous and anatase phases prepared by this method exhibited higher photocatalytic activities than the other samples. This shows that the amorphous phase also plays a role in reducing electron−hole pair recombination. The amorphous-to-anatase and anatase-to-rutile phase transformations in nanocrystalline TiO_2 take place with increasing temperature and showed a red shift of 35.5 nm in NCT-913 as compared to NCT-393. Nanocrystalline TiO_2 is thermally stable in the anatase form to 833 K. The lowest band gap, 3.01 eV, was obtained at 1023 K, which contained the rutile phase. The anatase-to-rutile transition takes place in the temperature range of 833−913 K and is completed at 1023 K. The crystallite size increased by a factor of 3 as the temperature was increased from 393 to 1023 K. Finally, it was concluded that the photocatalytic degradation of nitrobenzene under UV light irradiation using synthesized nanocrystalline TiO_2 containing predominantly the anatase phase with a high surface area and low-energy band gap and with air purging is faster than that using P-25 Degussa.

Acknowledgment

The authors thank the Council of Scientific and Industrial Research, New Delhi, India, and Dr. P. K. Ghosh, Director of CSMCRI, for financial assistance and support. The authors are also thankful to Dr. Pragnya Bhatt, Mr. Jince Sebastian, Mr. C. K. Chandrakanth, and Mr. Shobhit Singh Chauhan for analytical support and Dr. K. H. Modi for COD measurement assistance.

Literature Cited

(1) Haigler B. E.; Spain, J. C. Biotransformation of nitrobenzene by bacteria containing toluene degradative pathways. *Appl. Environ. Microbiol.* **1991**, 57(11), 3156−62.

(2) *Agency for Toxic Substances and Disease Registry (ATSDR). Toxicological Profile for Nitrobenzene*; Public Health Service, U.S. Department of Health and Human Services, Atlanta, GA, 1990; available at http://www.atsdr.cdc.gov/taxfaq.html (accessed Dec 1990).

(3) Chou, W. L.; Speece, R. E.; Siddiqi, R. H. Acclimation and degradation of petrochemical wastewater components by methane fermentation. *Biotechnol. Bioeng. Symp.* **1978**, *8*, 391−414.

(4) Hallas, L. E.; Alexander, M. Microbial transformation of nitroaromatic compounds in sewage effluent. *Appl. Environ. Microbiol.* **1983**, *4*, 1234−1241.

(5) Canton, J. H.; Slooff, W.; Kool, H. J.; Struys, J.; Pouw, T. J.; Wegman, R. C.; Piet, G. J. Toxicity, biodegradability, and accumulation of a number of Cl/N-containing compounds for classification and establishing water quality criteria. *Regul. Toxicol. Pharmacol.* **1985**, *5*, 123−131.

(6) Barth, E. F.; Bunch, R. L. *Removability, Biodegradation and Treatability of Specific Pollutants*; Report EPA-600/g-79-034; U.S. Environmental Protection Agency, U.S. Government Printing Office: Washington, DC, 1979.

(7) Davis, E. M.; Murray, H. E.; Liehr, J. G.; Powers, E. L. Basic microbial degradation rates and chemical byproducts of selected organic compounds. *Water Res.* **1981**, *15*, 1125−1127.

(8) Korte, F.; Klein, W. Degradation of benzene in the environment. *Ecotoxicol. Environ. Saf.* **1982**, *6*, 311−327.

(9) Lutin, P. A.; Cibulka, J. J.; Malaney, G. W. Oxidation of selected carcinogenic compounds by activated sludge. *Purdue Univ. Eng. Extens. Ser.* **1965**, *118*, 131−145.

(10) Marion, C. V.; Malaney, G. W. Ability of activated sludge microorganisms to oxidize aromatic organic compounds. *Purdue Univ. Eng. Extens. Ser.* **1963**, *115*, 297−308.

(11) Rodriguez, M.; Timokhin, V.; Michl, F.; Contreras, S.; Gimenez, J.; Esplugas, S. The influence of different irradiation sources on the treatment of nitrobenzene. *Catal. Today* **2002**, *76*, 291−300.

(12) Lipczynska-Kochany, E. Degradation of nitrobenzene and nitrophenols by means of advanced oxidation processes in a homogeneous phase: Photolysis in the presence of hydrogen peroxide versus the Fenton reaction. *Chemosphere* **1992**, *24*, 1369−1380.

(13) Contreras, S.; Rodriguez, M.; Chamarro, E.; Esplugas, S. UV- and UV/Fe(III)-enhanced ozonation of nitrobenzene in aqueous solution, *J. Photochem. Photobiol. A: Chem.* **2001**, *142*, 79−83.

(14) Kamble, S. P.; Sawant, S. B.; Pangarkar, V. G. Novel solar based photocatalytic reactor for degradation refractory pollutants. *AIChE J.* **2004**, 71648−1651.

(15) Bhatkhande, D. S.; Kamble, S. P.; Sawant, S. B.; Pangarkar, V. G. Photocatalytic and photochemical degradation of nitrobenzene using artificial ultraviolet light. *Chem. Eng. J.* **2004**, *102*, 283−290.

(16) Bhatkhande, D. S.; Pangarkar, V. G.; Beenackers, A. A. C. M. Photocatalytic degradation of nitrobenzene using titanium dioxide and concentrated solar radiation: chemical effects and scale-up. *Water Res.* **2003**, *37*, 1223−1230.

(17) Alfano, O. M.; Bahnemann, D.; Cassano, A. E.; Dillert, R.; Goslich R. Photocatalysis in water environments using artificial and solar light. *Catal. Today* **2000**, *58*, 199−230.

(18) Hoffmann, M. R.; Martin, S. T.; Choi, W.; Bahnemann, D. Environmental Applications of Semiconductor Photocatalysis. *Chem. Rev.* **1995**, *95*, 69−96.

(19) Fox, M. A.; Dulay M. T. Heterogeneous Photocatalysis. *Chem. Rev.* **1993** *93*, 341−357.

(20) Litter, M. I. Heterogeneous photocatalysis: Transition metal ions in photocatalytic systems. *Appl. Catal. B: Environ.* **1999**, *23*, 89−114.

(21) Mills, A.; Hunte, S. L. An overview of semiconductor photocatalysis. *J. Photochem. Photobiol. A: Chem.* **1997**, *108*, 1−35.

(22) Balasubramanian, G.; Dionysiou, D. D.; Suidian, M. T.; Subramanian, Y.; Baudin, I.; Laîné, M. Titania Powder Modified Sol−Gel Process for Photocatalytic Applications. *J. Mater. Sci.* **2003**, *38*, 823−831.

(23) Kim, D. H.; Anderson, M. A.; Zeltner, W. A. Effects of Firing Temperature on the Photocatalytic and Photoelectrocatalytic Properties of TiO_2. *J. Environ. Eng.* **1995**, *121*, 590−594.

(24) Li, W.; Ismat Shah, S. Structure and size distribution of TiO_2 nanoparticles deposited on stainless steel mesh. *J. Vac. Sci. Technol. B* **2002**, *20*, 2303.

(25) *ICDD Reference Pattern Database*; Joint Committee. on Powder Diffraction Standards, International Centre for Diffraction Data (JCPDS-ICDD): Newtown Square, PA, 1996; File 46.

(26) Spurr, R. A.; Myers, H. Quantitative Analysis of Anatase−Rutile Mixture with an X-ray Diffractometer. *Anal. Chem.* **1957**, *29*, 760−762.

(27) Cullity, B. D.; Stock, S. R. *Elements of X-ray Diffraction*, 3rd ed.; Prentice Hall: Upper Saddle River, NJ, 2001.

(28) Gregg, S. J.; Sing, K. S. W. *Adsorption, Surface Area and Porosity*, 2nd ed.; Academic Press: New York, 1982.

(29) Gratzel, M. *Heterogeneous Photochemical Electron Transfer*; CRC Press: Boca Raton, FL, 1988.

(30) Wang, W.; Gu, M.; Jin, Y. Effect of PVP on the photocatalytic behavior of TiO_2 under sunlight. *Mater. Lett.* **2003**, *57*, 3276−3281.

(31) Zielinska, B.; Morawski, A. W. TiO_2 photocatalysts promoted by alkali metals. *Appl. Catal. B: Environ.* **2005**, *55*, 221−226.

(32) Kim, E. J.; Hahn, S.-H. Microstructural changes of microemulsion-mediated TiO_2 particles during calcination. *Mater. Lett.* **2001**, *49*, 244−249.

(33) Chen, Y.-F.; Lee, C.-Y.; Yang, M.-Y.; Chiu, H.-T. The effect of calcination temperature on the crystallinity of TiO_2 nanopowders. *J. Cryst. Growth* **2003**, *247*, 363−370.

(34) Basca, R. R.; Kiwi, J. Effect of rutile phase on the photocatalytic properties of nanocrystalline titania during the degradation of p-coumaric acid. *Appl. Catal. B: Environ.* **1998**, *16*, 10−29.

(35) Zhang, B. Z.; Chen, B.; Shi, K.; He, S.; Liu, X.; Du, Z.; Yang, K. Preparation and characterization of nanocrystal grain TiO_2 porous mcrospheres. *Appl. Catal. B: Environ.* **2003**, *40*, 253.

(36) Wang, C. M.; Heller, A.; Gerischer H. Palladium catalysis of O_2 reduction by electrons accumulated on TiO_2 particles during photoassisted oxidation of organic compounds. *J. Am. Chem. Soc.* **1992**, *114*, 5230.

Received for review September 21, 2005
Revised manuscript received November 29, 2005
Accepted November 30, 2005

IE051060M